Environmental Science and Pollution Research (2023) 30:13671–13687
https://doi.org/10.1007/s11356-022-23004-w

RESEARCH ARTICLE

Prepared activated carbon from hazelnut shell where coated nanocomposite with Ag^+ used for antibacterial and adsorption properties

Esra Altintig[1] · Birsen Sarıcı[2] · Sukru Karataş[3]

Received: 16 June 2022 / Accepted: 8 September 2022 / Published online: 22 September 2022
© The Author(s), under exclusive licence to Springer-Verlag GmbH Germany, part of Springer Nature 2022

Abstract

In this research, prepared activated carbon by H_3PO_4 from hazelnut shells was coated with silver ions for the preparation of nanoparticles which were mixed in two ratios (1:0.5 and 1:1) by using of chemical reduction method. The adsorption capacity of activated carbons has been proven by BET and iodine number. Then, the antimicrobial effect of nanoparticles on the *Staphylococcus aureus* and *Escherichia coli* was investigated; in addition to that, the characterization of hazelnut shell and silver-coated activated carbons was determined by Brunauer–Emmett–Teller (BET), scanning electron microscope (SEM), Fourier transform infrared spectroscopy (FT-IR), and X-ray diffraction (XRD) methods. The optimum condition of activated carbon from hazelnut shells indicated that 66.01% carbon content within 36.22% efficiency, while BET surface area achieved as 1208 m2/g and its contained 0.6104 cm3 g^{-1} total pore volume. The microbial effect indicated that 105 CFU/mL of *E. coli* was completely inhibited in 30 min. Silver-coated activated carbon showed excellent bacteriostatic activity against *E. coli* and *S. aureus*. The results show that the composite has good prospects for applications in drinking water. *E. coli* of 10^4 CFU/mL in drinking water were destroyed within 25 min of contact with the filter made with AgAC.

Keywords Activated carbon · Chemical activation · Characterization · Hazelnut shell · Silver · Antibacterial effect

Resposible Editor: George Z. Kyzas

Novelty statement Activated carbons are used effectively in many environmental applications and first aimed to obtain activated carbon and then investigate the effectiveness of MB removal and the second stage, we applied antibacterial tests with silver-added activated carbons. We believe that this study will add innovation to the literature with its ease of use in water purification by examining the effect of antibacterial tests against time, which differs from other studies.

✉ Esra Altintig
altintig@subu.edu.tr

Birsen Sarıcı
b.sarici@hotmail.com

Sukru Karataş
karatassukru@gmail.com

[1] Pamukova Vocational School, Sakarya University of Applied Sciences, Sakarya 54900, Turkey

[2] Food Safety, and Nutrition Department, Food Safety Department, Istanbul Aydın University, Istanbul 34290, Turkey

[3] Department of Nutrition and Dietetics, Istanbul Arel University, Istanbul 34200, Turkey

Introduction

Activated carbon (AC) has a large inner surface area and carbon content and is an absorbent material with a long history and an unidentified structural formula. In the production of activated carbon, physical or chemical activation or a combination of these two methods can be used (Hameed et al. 2007). Physical activation is carried out by the formation of the solid product obtained because of the carbonization of the raw material by heat treatment with an oxidizing gas at a suitable temperature, (Danish et al. 2013). The suitable temperatures AC are used at 350–550 and 800–1100 °C for air, steam, and CO_2 respectively. The combination of low temperature, improved pore structure, and carbonization and activation processes in one system makes chemical activation advantageous. The preparation consists of two steps in chemical activation: carbonization and activation (Uner et al. 2021). The common activators in chemical activation include H_3PO_4, KOH, $ZnCl_2$, and K_2CO_3 (Morgan et al. 2009; Ucar et al. 2009; Angin 2014a). The obtained biomass-based AC is rich in surface functional groups

and shows impressive internal pore structure, facilitating its chemical and physical adsorption capacities. A high degree of microporosity over a wide area, unique surface chemistry, and large surface area are the main features that distinguish AC from other adsorbents (Benaddi et al. 2000; Gao et al. 2022). One of the most important factors in the use of agricultural products in the production of activated carbon is the high surface area of activated carbons obtained from agricultural products. In addition to these, one of the factors affecting the properties and quality of the AC to be obtained is the antecedent. In the literature, different types of precursors have been used for AC generation (Uner et al. 2021). In recent years, low-cost AC has been produced industrially from agricultural wastes such as almond shells, rice husk, apricot kernels, cherry kernels, coconut shells, and nutshell, Okra (Abelmoschus esculentus L.) (Altintig et al. 2015; Angin 2014b; Hayashi et al. 2002; Khuluk and Rahmat 2019; Uner et al. 2017). ACs produced from waste biomaterials are widely used for the removal of organic and inorganic impurities, water remediation, purification of noble metals, improvement of catalysis, and energy storage (Mohan et al. 2011; Uner et al. 2019). The economy of the adsorption process depends on the use of adsorbents, which are abundant, easily available, and have low production costs. Activated carbons are the most widely used adsorbents. However, the high demand has led the researchers to supply the starting raw material from renewable resources in the preparation of activated carbon (Mohan et al. 2011). For this reason, the production of activated carbon from cheap raw materials has gained importance. For this purpose, we aim to produce activated carbon from hazelnut shells, which are plentiful in our country and whose shells cannot be used adequately, to bring them into the economy (Gao et al. 2013). Considering the possible harmful effects of methylene blue dyestuff, the importance of removing dyestuffs from wastewater becomes more evident. Various physical, chemical, and biological methods are used for the treatment of wastewater. Adsorption, which is one of the chemical treatment methods, is one of the most preferred methods among the dyestuff removal techniques due to its insensitivity to toxic pollutants, ease of design and use, and low installation cost (Berrios et al. 2012). The pore size of activated carbons is one of the important criteria for removing these impurities. For example, if activated carbons with pore sizes larger than the volume of the MB molecule are used for the adsorption of methylene blue (MB), a cationic dye with a molecular volume of 371.07 $Å^3$ we used in our study, the MB adsorption capacity is expected to be higher in activated carbons with pore sizes smaller than the MB volume (Uner et al. 2019). The adsorption process is affected by the pH value of the aqueous solution, the nature of the dyestuff, and its substituent groups. In addition, the concentration and presence of surface functional groups play an important role in the dyestuff's adsorption capacity and removal mechanism (Altintig et al. 2022). The presence of carbonyl $(CO)_X$ and carboxyl $(COO)^-$ functional groups on the carbon surface determines the adsorption properties of activated carbon and significantly affects the adsorption properties as they act as catalysts (Kazemi et al. 2020).

Silver nanoparticle, one of the nanoparticles, has been widely used in various processes for many years due to their superior antibacterial properties and large surface area (Tuan et al. 2011). In addition, the production of silver nanoparticle-loaded materials attracts more attention because it has the lowest toxic effect on human health when compared to nanoparticles of other metal ions (Yang et al. 2009). Silver-containing nanoparticles are usually prepared by chemical reduction. $AgNO_3$ is used as a metal precursor in this process, and hydrate is used as a reducing agent (Chaudhari et al. 2007). The shape and size of silver nanoparticles are important parameters in this synthesis. The size of silver nanoparticles is affected by the temperature of the solution, the concentration of metal salts, the reducing agent, and the reaction time. Silver nanoparticles are used in many fields such as catalysis, optics, and microelectronics (Dang et al. 2011).

AC can be used as an ideal support material for silver nanoparticles due to its high surface area and pore volume. In addition, since the biocompatibility of AC with microorganisms can increase the proliferation of bacteria, the bonding of silver nanoparticles to activated carbon is advantageous in terms of providing antibacterial properties (Zhang et al. 2015). By bonding silver nanoparticles to a support material to produce silver nanoparticle-doped adsorbent, agglomeration of nanoparticles can be prevented, and their recycling and reuse can be achieved (Kazmi et al. 2014). Due to nanoparticles' different physical and chemical properties, it has started to find a wide application area. Most of the nanoparticle atoms are surface unsaturated and can easily bind other atoms. Nanoparticles have high sorption capacity due to a lack of internal diffusion resistance and large surface area (Zhang et al. 2016). By bonding nanoparticles to activated carbon, which has a porous structure, it is possible to obtain an adsorbent with a much larger surface area. Thus, the adsorption capacity of AC is further increased. Many studies show antibacterial properties when silver is added to these nanoparticles. Because silver nanoparticles exhibit bactericidal ability, especially against *Staphylococcus aureus* and *Escherichia* coli (Kumar et al. 2008), they have been adopted in the production of commercial products.

Escherichia coli (*E. coli*) is one of the gram-negative bacilli from the enteric bacteria group living in the normal intestinal flora. Rod-shaped bacteria are 1–2 μm long and 0.1–0.5 μm in diameter. Since it normally lives in the

intestine, the presence of *E. coli* in environmental waters and food is a sign of fecal contamination, and in this respect, *E. coli* is an important indicator of food safety.

Staphylococcus aureus (*S. aureus)* is a gram-positive bacterium found as a member of the normal microbiota in humans in the upper respiratory tract, intestinal mucosa, and skin. *S. aureus*, which can normally colonize the skin but can cause serious infections, is a microorganism that is frequently seen with methicillin-resistant (MRSA) strains, especially in hospital infections, and has high mortality rates. Methicillin-resistant *Staphylococcus aureus* (MRSA) is an important pathogen for food safety and is of increasing importance in hospitals as well as in society and livestock (Wu et al. 2019; Hassan et al. 2017).

E. coli is a bacterium that lives in microaerobic conditions and exhibits aerobic and anaerobic metabolism. The World Health Organization reported that the most common microorganism among waterborne pollutants is *E. coli* and its adverse effects on health. According to the report, *E. coli* is an important pathogen that is more persistent in water, less resistant to chlorine, and highly contagious but carries a high risk for health problems (Hulton G and World Health Organization 2012; Unicef 2017).

AC is frequently used in water treatment to remove organic and inorganic pollutants due to its high adsorption ability, specific surface reactivity, and high surface area. However, due to the biocompatibility of AC used to purify drinking water, it is an environment where bacteria can adhere and grow and live. In such a case, there is a risk of re-contaminating the water while ensuring the disinfection of the water. Antibacterial ACs are necessary to eliminate this risk. The antibacterial effects of metallic silver have been known for centuries (Zhao et al. 2013).

This research aims to prepare activated carbon by H_3PO_4 from hazelnut shells and to coate with silver in order to prepare nanoparticles. The proposed roadmap and treatment methodology will be in line with the principles. Helps maintain and strengthen the circular economy. With the concept of zero waste, the advancement of global food security and the protection of the environment, while contributing to the sustainability of the agricultural product sector. In addition to that investigating the properties of nanoparticles by XRD, FT-IR, SEM/EDS, and BET analysis methods and determining the antimicrobial effect of nanoparticles on the *Staphylococcus aureus* and *Escherichia coli*.

Materials and methods

Materials

The raw hazelnut shell was collected from Giresun (Turkey) and was used in the production of AC. Sodium alginate, H_3PO_4, $AgNO_3$ (purity > 99%), sodium hydrazine monohydrate, HCl, and NaOH chemicals used in the study were supplied from Merck (Germany). All chemicals are analytical reagent grade.

Preparation of the activated carbons

The first stage of the study aimed to produce AC from HS by the chemical activation method. First, the collected nutshells were dried at room temperature. These materials were thereafter washed several times with distilled water and dried. Air-dried HS were ground and sieved to determine the average particle diameters. This study produced AC from HS by chemical activation and carbonization methods. H_3PO_4 was used for chemical activation.

Activated carbons were synthesized to study activation temperatures (600, 700, and 800 ◦C) and different chemical impregnation ratios (HS /H_3PO_4) 1/1, 1/2, 1/3. First of all, the adsorption properties of the synthesized AC were tested using the Iodine number. As a result, AC with the highest iodine adsorption capacity was used in the continuation of the experimental studies.

In the experiments, the dried HS /H_3PO_4 ratio was determined as 1/1. The HS sample and the chemical mixture were mixed in a magnetic mixer for 24 h and the chemical substance was impregnated into the HS. The samples were then filtered and dried overnight in an oven at 103 °C (± 3 °C). The chemically impregnated sample was carbonized at 800 °C at a heating rate of 10 °C min^{-1} under a flow of 100 mL min^{-1} nitrogen (N_2) gas for 1 h at a temperature of 100 °C. After the carbonization temperature reached the maximum value, the sample was kept at the same temperature for 1 h. At the end of this period, the system was allowed to cool to room temperature (Altintig et al. 2013). AC was washed with 1 M HCl solution to remove the remaining H_3PO_4 compounds. Thereafter, they were washed several times with hot and, finally, cold distilled water until the pH reached 6–7. After that, the solid product was repeatedly washed with deionized water and then dried at 105 ± 5 °C for 24 h to obtain AC. The yield of the products was calculated by Eq. (1). The yield of AC (%) was determined by the weight of the AC obtained because of carbonization The yield was subjected to the carbonization process.

$$\text{Yield of AC (wt\%)} = \frac{\text{Final weight of AC}}{\text{Initial weight of HS}} \times 100 \quad (1)$$

Sample characterization

The experimental studies carried out all mixing processes with the Wisestir MSH-20A magnetic stirrer. Quantity measurements were made with a Precisa XB 220A test

balance. The pH values of the solutions were measured with a Mettler TOLEDO brand Seven Compact model device. The carbonization process of activated carbon was carried out with Proterm (PTF 12) tube furnace. The purified water used in the experiments was obtained from the Nuve NS112 device. Nuve SL 350 brand shaker was used in shaking processes. Mido/2/AL brand was used in oven drying processes. Wet chemical analyzes, ash, and moisture determinations were made in the Nuve MF 100 brand oven. In addition, the functional groups of HS, AC, and silver added activated carbons were determined using a Fourier transform infrared spectroscopy (FT-IR) device (PERKIN ELMER UATR-TWO diamond ATR brand) in the wavelength range of 4000–400 cm^{-1}. In the determination of the crystal structures of AC and silver-added activated carbons, measurements were made with the Rigaku brand device XRD. Scanning Electron Microscopy (SEM, Jeol JSM-6060 LV device) was used to determine the surface morphology. Multi-point Brunauer–Emmett–Teller (BET) surface area (m^2 g^{-1}), pore size (nm), micropore and Meso-macropore volumes (cm^3/g) using surface and pore characterization device (S_{BET}) analysis was determined by the nitrogen (N_2) gas adsorption technique in a liquid nitrogen environment at 77 K. Before the BET analysis, the temperature in the degassing treatment applied to the sample was 300 °C and the time was 360 min.

The iodine number calculation method was used to determine the adsorption capacity of activated carbons. The iodine number is a measure of microporosity. The iodine number of activated carbon was determined using the sodium thiosulfate volumetric method (mg iodine/g activated carbon) (ASTM D 4607–94, 2006). The iodine number was determined according to the ASTM D4607-94 method.

The MB adsorption studies and the AC sample measurements were made in the Shimadzu UV-2600 brand UV device, at a wavelength of 665 nm determined for its MB. The capacity of large pores of activated carbon can be determined by MB adsorption. 100 mg L^{-1} MB solution. 0.1 g of AC was weighed and added 100 mL of 100 mg L^{-1} MB solution was added. The mixtures were shaken in an orbital shaker for 24 h. Then, the mixture was centrifuged at 1200 rpm and the solid and liquid parts were separated subsequently. It was measured by a UV–Vis spectrophotometer and The MB adsorption capacity of ACs was calculated with the Eq. (2).

$$qe = \frac{(Co - Ce)}{m} xV \tag{2}$$

V (L) is the solution volume, m (g) is the adsorbent dose used in adsorption (activated carbon), and C_0 and Ce are the initial and the final concentration (mg L^{-1}), respectively.

AC/Ag preparation of the mixtures

In this study, silver nitrate ($AgNO_3$) was used for preparation as a precursor to form silver nanoparticles due to that 25% by weight NH_3 and solid $AgNO_3$ were mixed at two different concentrations (1 g and 0.5 g) in a 100-mL beaker. The mixture was stirred for 60 min at room temperature (298 K) in a magnetic stirrer at 150 rpm in order to prepare the homogeneous mixture. The obtained biaminsilver nitrate ($[Ag(NH_3)_2]NO_3$) solution was stored in light-proof glass bottles covered with aluminum foils. The pH of the solution was adjusted to pH 9.0 with HNO_3 solution then the activated carbon sample was activated one-to-one (1 g:1 g) with sodium alginate (Sigma Aldrich) mixed in a magnetic stirrer at 200 rpm at room temperature for 60 min (Altintig and Kirkil 2016) later the hydrazine monohydrate was dropped into the solution. This study was mixed and carried out under nitrogen gas flow (200 min mL^{-1}) to provide an inert atmosphere. The mixture was stirred on a magnetic stirrer at room temperature for 4 h afterward obtained mixtures were filtered and washed with ethanol and distilled water then dried in an oven at 60 °C overnight. As a result of the process, Ag^+ ions in the silver metal were reduced to Ag + ions using hydrazine monohydrate reductant (Yang et al. 2009). The activation AC/Ag° mixtures are mixtures of AC and Ag^+ prepared with H_3PO4 at a rate of 1/1 for 24 h at 800 °C with weight ratios of AC: $AgNO_3$ equal to 1:0.5 and 1:1.

MB adsorption studies of activated carbon and silver-bonded activated carbons

To examine the effects of initial MB concentration on dyestuff removal, batch adsorption studies of activated carbon and silver nanoparticle bonded activated carbons were carried out. All experiments were performed with 0.1 g of activated carbon or silver nanoparticle bonded activated carbon and 100 mL of MB (50, 100, 150, 200, 250, 300 mg L^{-1}) solution at pH 7 and 25 °C. The mixtures were filtered with blue band filter paper and the supernatant phases were analyzed at 665 nm with a UV–vis spectrophotometer in order to determine the MB concentrations at equilibrium.

Antibacterial analysis

Microorganism cultures used in the experiments *E. coli* (ATCC 10,536) and *S. aureus* (ATCC 6556) were obtained from Istanbul Aydın University Food Processing Laboratory. The disk diffusion method was preferred to control the microbial properties of the obtained nanosilver-coated activated carbons. *E. coli* (ATCC 10,536) and *S. aureus* (ATCC 6556) and two different antibiotics discs (Ampicillin 10 mg, Cefotaxim 30 mg) were used for control purposes

on 2 different bacteria. In the study, a non-selective PCA medium (Plate Count Agar (Merck 1.05463) was used for the passage of microorganisms, and an MHA (Müller Hilton Agar Merck 1.05437) medium was utilized for the disk diffusion experiment. Cultures were allowed to grow on a non-selective medium CA passaged at 36.5 °C for 24 h, and then isolated colonies were selected and prepared inoculum (using ready-made saline). All the work was carried out in a burner flame environment, in order to achieve sterilization value. A few of the colonies of the bacteria showed similar morphology. Grain was taken with the help of a sterile cotton swab and suspended in sterile saline (0.85% NaCl) (SF). The density of the suspension was adjusted to equal to the McFarland 0.5 standard, corresponding to approximately $1–2\times10^8$ CFU/mL of *E. coli*. The 0.5 McFarland setting was checked each time using of the Thermo Multiskan Go photometric device. A sterile cotton swab was dipped into the inoculum suspension with a density adjusted to 0.5 McFarland, and the excess liquid in the cotton was discarded by pressing the cotton part of the swab against the tube wall and rotating it. The inoculum on the cotton was spread evenly all over the agar surface in three directions with the help of a stick. Antibiotic discs were used and stored at the manufacturer's suggestion. Petri was divided into 5 equal spaces, taking into account EUCAST (European Committee for Antimicrobial Susceptibility Testing) disc diffusion guidelines, and wells were drilled into each marked section with a sterile cork drill, 6 mm in diameter. Ten milligram nanosilver-coated activated carbons were placed in the opened wells. For comparison, antibiotic discs were placed on the agar surface within 15 min after inoculation. Plates inoculated with bacterial suspension and antibiotic discs were incubated for 24 h at 36.5 °C within 15 min. In plates deemed suitable for examination, bacteria were categorized as "susceptible," "resistant," or "intermediate susceptibility" for a specific antibiotic using EUCAST disc diffusion breakpoint tables in terms of quality control limits for the diameters of the zones of inhibition.

Removal of E. coli from drinking water by smear plate method using activated carbon coated with silver nanoparticle

AgACs, which were prepared in advance for use in the experiments and stored in light-proof sample containers, were sterilized in an oven at 110 °C for 6 h to remove possible microorganisms. One milliliter sample taken from the prepared suspension was transferred to 10 mL sterile saline and the suspension was diluted. After this process was repeated 3 times, corresponding to approximately $1–2\times10^5$ CFU/mL of *E. coli*, this time 20 mg of AgNPAC was added to 105 CFU/mL suspension and incubated at room temperature in an oxygenated environment at 150 rpm in a way that no AgNPAC granules would precipitate. The first moment of the mixing queue was accepted as 0 min, and then a 0.1-mL sample taken from the suspension was transferred to PCA medium at 10-min intervals. With a disposable sterile drigalski spatula, smear seeding was made to show a homogeneous distribution on the entire Petri surface. Sowings were done made at five different time intervals (0–10-20–30-40) then they were min was incubated at 37 °C for 24 h and the results were evaluated by colony counting (Yoon et al. 2008; Biswas and Bandyopadhyaya 2016).

Result and discussion

Preliminary analysis studies of hazelnut shell and activated carbon

The main reason why we chose the chemical H_3PO_4 in chemical activation in our study is that it is frequently preferred due to its lower toxic effects on the environment, cheaper, more effective activation, and lowering carbonization temperature compared to other activating agents (such as $ZnCl_2$, KOH or NaOH) in the literature research (Sych et al. 2012; Al Bahri et al. 2012).

Proximate and ultimate analysis experiments of HS used in the production of AC and activated carbon impregnated with H_3PO_4 at a ratio of 1:1 were carried out. Analysis results are given in Table 1.

Table 1 presents the characteristic properties of HS and AC obtained from its activation with H_3PO_4. Raw materials with low ash, high volatile matter, and fixed carbon content are preferred in the production of AC. When the studies in the literature are examined, it has been observed that vegetable wastes with volatile matter content between 20.40 and 67.36%, fixed carbon content between 17.62 and 70.70%,

Table 1 Characteristics of the HS and AC

Characteristics	Methods	HS	AC
Moisture content (wt.%)	ASTM D 2016 2.67	7.23	2.87
Proximate analysis (wt.%)		64.91	9.1
Volatile Matter	ASTM E 872 78.50	26.56	86.83
Ash	ASTM D1102 0.17	1.3	1.2
Fixed carbon	By difference		
%Yield		-	36
Ultimate analysis (wt.%)			
Carbon	AR2092-0721	49.35	56.01
Hydrogen		6.10	3.44
Nitrogen		0.36	0.77
Sulfur		0.048	0.012
Oxygen	By difference	44.142	39.768

*Fixed carbon = 100-(moisture + ash + volatile matter)

and ash content between 0.3 and 5.0% are used in the production of activated carbon (Hadoun et al. 2013; Budinova et al. 2006). In this context, according to the results of the short analysis of the raw materials in our study, it was concluded that the HS activated with 1:1 H_3PO_4 has low ash content (1.3%), volatile matter (64.91%), and fixed carbon (26.56%), and it is a suitable raw material for the production of AC from HS.

When the preliminary analysis results of AC are evaluated in Table 1, it is seen that the amount of ash, moisture, and volatile matter determined in the hazelnut shell decreased as expected in the AC, while the fixed carbon ratio increased.

The yield of hazelnut shell activated with H_3PO_4 at a ratio of 1:1 was found to be 36%. A similar trend has been reported in the literature (Hadoun et al. 2013; Yorgun and Yıldız 2015; Prahas et al. 2008).

The contents of carbon, hydrogen, nitrogen, and sulfur of the HS and AC were measured using a LECO CHNS 628 Elemental Analyzer with ± 0.4% accuracy (LECO Instruments, USA). The oxygen contents were calculated by difference. The elemental composition of AC and HS samples is given in Table 1. When the HS and AC elemental analysis results are compared, it is seen that the amount of carbon contained in AC increases with carbonization.

N_2 adsorption/desorption analysis of AC and silver coated ACs

Based on the nitrogen gas (N_2) adsorption method in a liquid nitrogen atmosphere, the results of the BET isotherms of activated carbon and silver coated ACs obtained by the activation of the HS with H_3PO_4 were measured.

The surface areas, iodine number, MB number, t-Plot micropore area, total porosity area, microporosity volume, average pore size, pore-volume, and pore size properties of AC and silver-coated ACs are given in Table 2 comparatively.

According to a classification made by IUPAC, a pore size greater than 500Å is called a macropore, between 500 and 20Å is called a mesopore, and less than 2Å is called a micropore (Saeed et al. 2003). In our study, the pore size of AC was found to be 20.211 Å. This tells us that our AC is a mixture of micro and mezzo.

ACs are generally solids with dense aromatic groups, large surface area, and pore volume. The pores in the carbon cause an increase in the surface area after activation (Mbarki et al. 2022). Surface area is one of the important properties of activated carbon to be used for adsorption. The size of the surface area means that the pore volume that will perform the adsorbing is also large. This porosity is a requirement for the effective use of activated carbon. Although the surface area of activated carbons used commercially in the literature is in the range of 400–1000 $m^2\ g^{-1}$, this value can be exceeded in special-purpose productions (Lima et al. 2019; Spessato et al. 2019). Looking at Table 2, the BET surface area value of activated carbon obtained by chemical activation of H_3PO_4 was measured as 1208 $m^2\ g^{-1}$. This result shows us that the surface area of our activated carbon is large enough. 1142 mg g^{-1}, which we found because of iodine adsorption, is quite compatible with this result. The high iodine adsorption indicates that our AC is generally microporous.

When Table 2 is examined, it is seen that the surface area, micropore area, outer surface area, micropore volume, and average pore size decrease as the amount of silver added to the activated carbon increases. Chen et al. 2000, in their study on activated carbon fibers, showed that the antibacterial effect increased as the surface area decreased (Feng et al. 2000). Yang et al. 2009, showed that the surface area of silver nanocomposites prepared by adding silver to bamboo charcoal decreased as the amount of added silver increased (Yang et al. 2009).

While the macropores allow the molecule to be absorbed and transferred to the AC, the meso and micropores perform the adsorption process. Mesopores are crucial for the absorption of organic compounds (Jiun-Horng et al. 2008; Fischer et al. 2017; Ng et al. 2018; Zhang et al. 2009). In our study, it is seen in Table 2 that the pore size increased after adding Ag to the AC. The increase in the amount of silver and the size of the mesopores can be explained by the increase in its antibacterial effect (Hadoun et al. 2013). The pore width is in the range of 20.211–24.787 Å as seen in Table 2 of this study.

These results show us that the AC we have obtained can be used effectively in the removal of organic compounds such as MB.

Table 2 Textural properties of AC and Ag impregnated ACs

Samples	S_{BET} (m^2/g)	*t-Plot Micropore* (m^2/g)	*t-Plot* (m^2/g)	V_{total} (cm^3/g)	V_{micro} (cm^3/g)	*Average pore size* (Å)	*Iodine number, mg/g*
AC	1208	534.0068	674.0041	0.6104	0.254	20.211	1142
AC/Ag-0.5	1185	444.6077	740.311	0.6847	0.210	23.115	-
AC/Ag-1.0	899.933	301.8536	598.079	0.5576	0.155	24.787	-

Iodine number (IS) determination provides information about the surface area of activated carbons due to its ability to adsorb small molecules and is an indicator of porosity (Saka and Balbay 2021). In our study, the iodine number was calculated as 1142 mg g^{-1} (Table 2). The iodine number we found showed parallelism with the surface area of the AC. The high iodine number given in the literature is generally between (500 and 1200 mg g^{-1}) (Benaddi et al. 2000). Our study is among these values. This result shows that AC synthesized with H_3PO_4 activation has a high ability to adsorb impurities and a high microporosity of activated carbon.

Textural characterization by SEM

SEM and EDS images of HS, AC, AC/Ag-0.5, and AC/Ag-0.1 samples are shown in Fig. 1a-d , respectively.

SEM photographs of hazelnut shells are shown in Fig. 1a HS has a fibrous appearance. These fibers are visible in SEM images. When SEM–EDS results are examined, C, O, Na, Ca, K, and Cu elements were found in the structure. It is thought that these elements come from the soil and hazelnut's structure.

SEM photographs of activated carbon are shown in Fig. 1b. When this photograph was examined, significant differences were observed between the surface topography

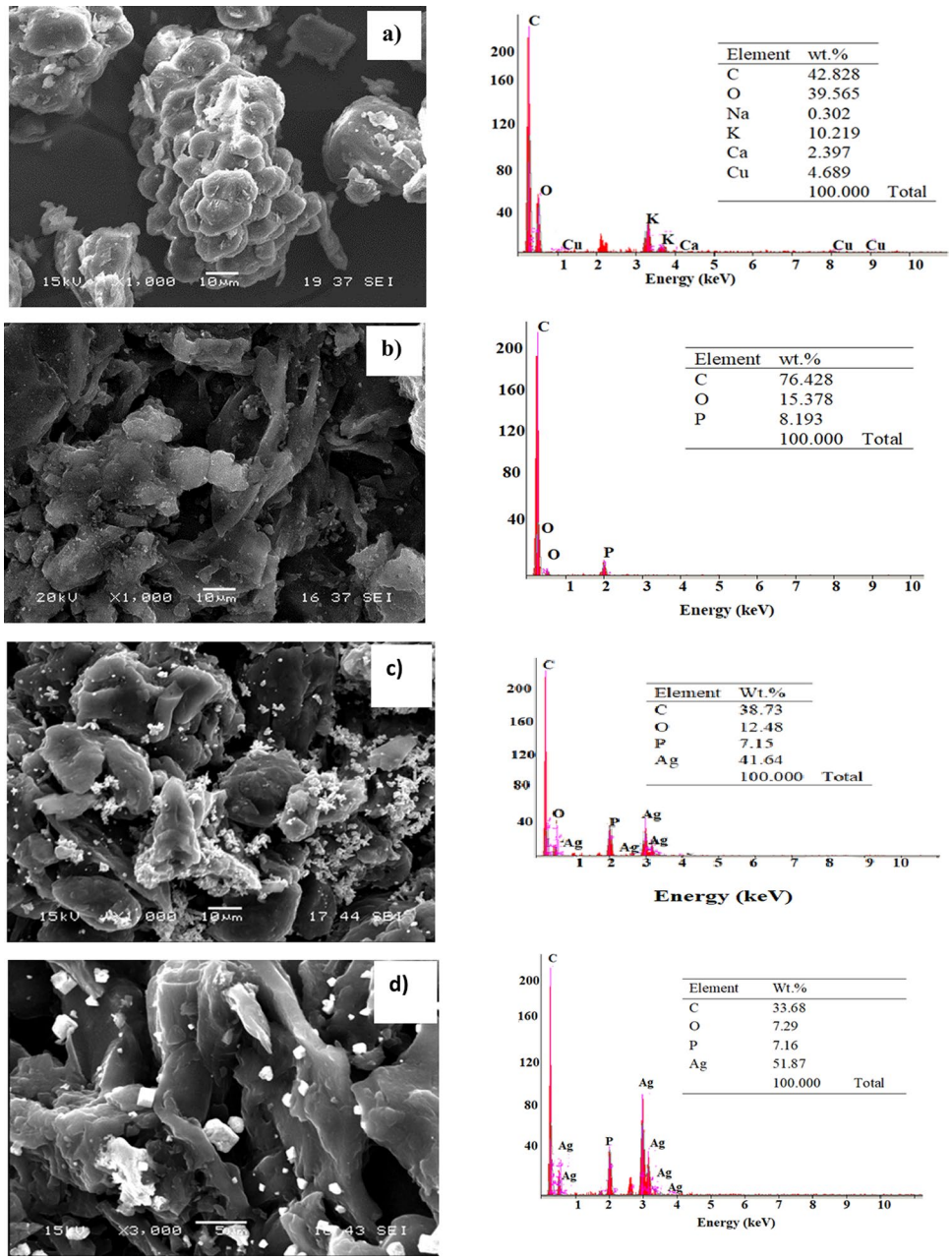

Fig. 1 SEM and EDS **a**) hazelnut shells, **b**) activated carbon **c**) of AC impregnated with 0.5 g Ag, **d**) of AC impregnated with 1.0 g Ag

of the HS and ACs. While there are no pores on the surface of the raw HS, many large pores have developed on the surface of the ACs. Depending on the impregnation ratio, the outer surfaces of AC have pores of different sizes and shapes. Similar results have been reported in the literature (Hadoun et al. 2013; Wang et al. 2005). When the EDS analysis was examined, C, O, and P elements were found on the surface of the activated carbons. Although C and O are the elements that should be in the activated carbon, it has been determined that there is phosphorus on the surface. It has been determined that the phosphorus on the surface of the activated carbon comes from the phosphoric acid residues that remain in the activated carbon during the activation process and cannot be removed by washing.

Figure 1c and d shows SEM photographs after silver bonding to activated carbon. It is seen that the surface morphology of the AC and silver-coated ACs changed. As the amount of silver increases, the whiteness on the surface increases. It is seen from the images that activated carbon with a 24-h impregnation time adsorbs silver. It is seen that the AC we obtained has a porous structure and due to its high surface area, it binds silver at a high rate (Altıntıg and Kirkil 2016; Yang et al. 2009). When the amount of Ag added increases from 0.5 to 1.0 g, it is seen that the amount of silver increases. Moreover, according to the SEM results, as the silver ratio increases from 0.5 to 1.0 g, the amount of silver added to the surface also increases.

When the EDS analyzes are examined (Fig. 1a), it is seen that the hazelnut shell mainly contains C (42.828) and O (39.565). This ratio revealed that AC consists of C (76.428%) and O (15.378%) elements. C ratio increased in activated carbon. This shows us that there is activation. However, in the EDS analysis of 0.5 g Ag-ACs (Fig. 1c), the element ratios for C, O, and Ag were 38.73%, 12.48%, and 41.64%, respectively. In Fig. 1, the amount of Ag increased to 51.87% in 1.0 g of Ag-impregnated activated carbon. This result shows that the silver nanoparticles are successfully attached to the AC surface.

Powder XRD study

With XRD, important data are obtained about the composition of the inorganic substance in the structure. Figure 2a-d gives a comparative XRD plot of hazelnut shell, activated carbon, AC/Ag-0.5, and AC/1.0 samples, respectively.

With XRD, important data are obtained about the composition of the inorganic substance in the structure. Figure 2a-d a comparative XRD graph of the samples of HS, AC, AC/Ag-0.5, and AC/1.0 materials, respectively.

Figure 2a-b shows the XRD spectrum of the HS and AC sample, respectively. Weak peaks of 22° and 44° were observed in these spectra. These weak peaks indicated that the HS and AC had an amorphous structure and there is no characteristic peak after activation. Similar results were reported in the literature (Altintig et al. 2013, Altıntıg et al. 2015; Saka and Balbay 2021).

In Fig. 2c-d, the XRD spectra of AC/Ag-0.5 and AC/Ag-1.0 samples prepared from AC obtained by impregnation with H_3PO_4 for 24 h (1/1) are shown. When the images are examined, the peaks supporting the presence of silver in the mixtures are seen. It is clear from the sharpness of the peaks that after the addition of silver, the amorphous structure of activated carbons turns into a crystalline structure. As a result of XRD analysis of AC with the silver nanoparticle, 38.28°; 44.46°; 64.54°; sharp peaks were obtained at 77.22° and 81.66°. These peaks obtained because of the analysis belong to surface-centered metallic silver in the coordinates (111), (200), (220), (311), (222). No silver oxide peaks were found in the structure in XRD results (Karadirek and Okkay 2019; Sang et al. 2016; Singh et al. 2014). This result leads us to the conclusion that silver is attached to activated carbon in the metallic form (Altintig et al. 2013). It is seen that the intensity of the characteristic peaks of silver increases as the amount of $AgNO_3$ added to the ACs increases. This suggests that silver pieces with larger crystals were formed. These results show parallelism with SEM results.

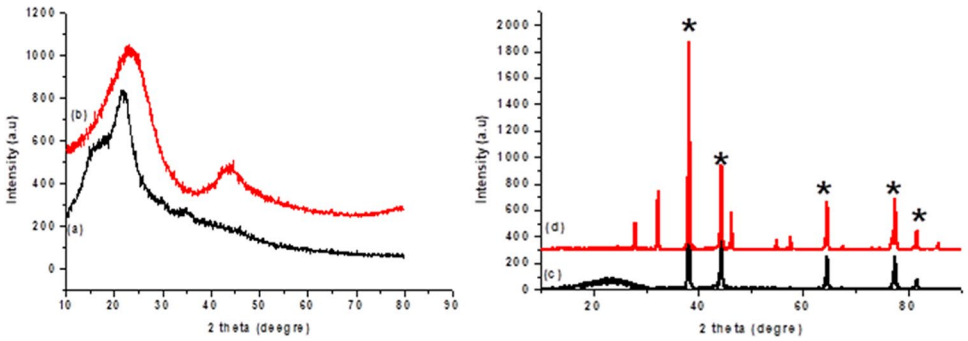

Fig. 2 XRD pattern of **a**) hazelnut shells, **b**) activated carbon, **c**) of AC impregnated with 0.5 g Ag, **d**) of AC impregnated with 1.0 g Ag

FTIR analysis

FTIR spectra were taken to determine the functional groups of HS, AC obtained by chemical activation of HS, and silver-coated activated carbon produced in two different ratios.

FTIR spectra were taken to determine the functional groups contained in the HS, the AC obtained by the chemical activation of the hazelnut shell, and the silver-coated activated carbon in two different ratios. FTIR spectra of HS are shown in Fig. 3a. Strong peaks at 3400 cm^{-1} were attributed to the OH stretching vibration of hydroxyl functional groups. The peaks at 2800 cm^{-1} were assigned to the stretching vibration of C-H bonds, and the peak at 1160 cm^{-1} represented the stretching vibration of the C = C bonds in the benzene ring. Bands in the region of 1104–998 cm^{-1} showed the presence of C-O, which was ascribed to alcohols, phenols, acids, or esters. The peak around 1050 cm^{-1} is due to R-OH groups (Hadoun et al. 2013). In addition, the band around 1690 cm^{-1} indicates C = O carbonyl groups. Peaks around 1500 cm^{-1} indicate $–CH_2=$ vibrations. Similar peaks were also observed in the literature (Mbarki et al. 2022; (Jawad et al. 2019). It can be easily observed that in Fig. 3, OH and other peaks disappeared this may be due to high-temperature activation and carbonization in ACs.

Figure 3c and d shows the comparative FT-IR spectrum of AC with 0.5 and 1.0 g of silver added samples, respectively. When silver is added to activated carbon, peaks of 1618 cm^{-1} and 1005 cm^{-1} and 2907 cm^{-1} appear. As the amount of silver increases, the sharpness of the peaks decreases. These peaks became apparent when silver was added, and the peaks 2907 cm^{-1}, 1618 cm^{-1}, and 1005 cm^{-1} were shown as the Ag^+ ion combines activated carbons by reduction (Singh et al. 2008; Altıntıg and Kirkil 2016).

Adsorption isotherm studies

The adsorption isotherm determines were carried out to evaluate the adsorption capacity of AC and Ag/AC for MB. A certain amount of AC and Ag/AC was added to 100 mL MB solution with the initial concentration ranging from 50 to 300 mg L^{-1}. The mixture was stirred at 250 rpm for 24 h at 298 K temperatures for adsorption. The adsorption properties of the samples were investigated by fitting isotherm models including Langmuir and Freundlich models. The Langmuir and Freundlich isotherms were widely used to study the relationship between the adsorption capacity and the equilibrium concentration of adsorbate under a certain temperature (Wu and Yu 2006, Dinu and Dragan 2010). The linear correlation of the Langmuir isotherm is given in Eq. (3).

$$\frac{C_e}{q_e} = \frac{1}{q_m K_L} + \frac{1}{q_m} Ce \tag{3}$$

Ce is the adsorbate concentration in the solution following the adsorption (mg L^{-1}), qe is adsorbed amount onto adsorbent (mg g^{-1}), and KL is the isotherm coefficient (L mg^{-1}), qmax is the maximum adsorption capacity of adsorbent (mg g^{-1}).

Equilibrium data calculated q_{max} as 277.77, 357.14, and 454.54 mg g^{-1} for AC, AC impregnated with 0.5 g Ag and AC impregnated with 1.0 g Ag, respectively.

Freundlich isotherm model assumes the multi-layer coating of the adsorbent surface by adsorbent molecules (Karadirek and Okkay 2019). This linear formulation has been submitted in formula (4) as follows.

$$lnq_e = lnK_f + \frac{1}{n} C_e \tag{4}$$

where q_e refers to the equilibrium concentration (mg g^{-1}) of adsorbate on the surface of the adsorbent, C_e refers to adsorbate (mg L^{-1}) in solution, and K_f and n refer to Freundlich's constants.

Isotherm parameters calculated by linear Langmuir and Freundlich isotherm models are given in Table 3.

In Table 3, where the Langmuir and Freundlich isotherm constants are given together, is evaluated, it shows that the correlation coefficient of the Langmuir isotherm is in the range ($R^2 = 0.99$) and the correlation

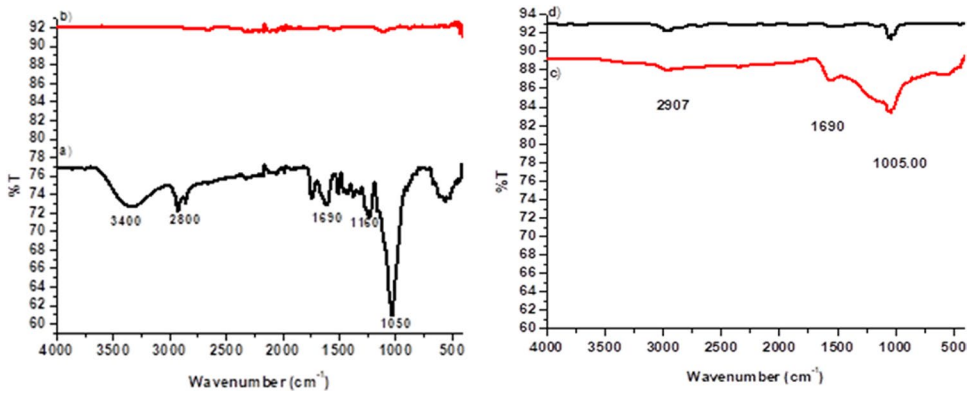

Fig. 3 FTIR spectrums of **a**) hazelnut shells, **b**) activated carbon, **c**) of AC impregnated with 0.5 g Ag, **d**) of AC impregnated with 1.0 g Ag

Table 3 Adsorption isotherm parameters for MB on AC and Ag impregnated ACs

Sample	Langmuir isotherm			Freundlich isotherm		
	q_m (mg/g)	K_L (L/mg)	R^2	K_F	n (l/mg)	R^2
AC	277.77	0.38	0.99	84.17	2.84	0.88
AC/Ag-0.5	357.14	0.08	0.99	37.12	1.69	0.93
AC/ Ag-1.0	454.54	0.05	0.99	27.80	1.45	0.98

coefficient of the Freundlich isotherm is between ($R^2 = 0.877–0.979$) (Fig. 4). Comparing the correlation coefficients, the Langmuir isotherm is best fitted to the adsorption model which proves that the MB was adsorbed by AC, AC impregnated with 0.5 g Ag and AC is given impregnated with 1.0 g Ag in a homogenous monolayer. The maximum adsorption capacities (q_{max}) of AC calculated from the linear Langmuir isotherm equation, AC impregnated with 0.5 g Ag and AC impregnated with 1.0 g Ag are 277.77, 357.14, and 454.54 mg g^{-1}, respectively. It can be seen from Fig. 5 that the experimental MB adsorption capacities (q_{max}) of silver-impregnated activated carbons are higher than the adsorption capacity of AC. According to the Freundlich isotherm, the n value of between 1 and 10 is known as adsorption fitness (Mishra and Patel 2009). This value is between 1.45 and 2.84 in all our samples which shows that it is suitable for MB adsorption. In addition, a high Kf value indicates high adsorption affinity. The q_{max} value is calculated for the highest 1.0 g Ag impregnated AC. This tells us that the highest adsorption capacity is 1.0 g Ag impregnated AC.

Kinetic studies

Pseudo-first- and second-order kinetic models were utilized to examine the adsorption kinetics and mechanism. Pseudo-first-order and pseudo-second-order models were used to investigate the kinetic adsorption of MB on AC, 0.5 and 1.0 g Ag-impregnated AC. The linear equations of pseudo-first-order and pseudo-second-order equations are as follows:

$$ln(q_e - q_t) = lnq_e - \frac{k_1}{k2}t \tag{5}$$

$$\frac{t}{q_t} = \frac{1}{k_2 q_e^2} + \frac{t}{q_e} \tag{6}$$

where k_1 (min^{-1}) the adsorption rate is calculated by linear regression analysis of the pseudo-first-order model from the slope of a linear plot of experimental data; k_2 (g mg^{-1} min^{-1}) is the constant of the pseudo-second-order rate; qe (mg g^{-1}) is the sorption capacity at equilibrium; qt (mg g^{-1}) is the adsorption capacity at time t (min). Kinetic data from pseudo-first- and second-order modeling of AC, 0.5

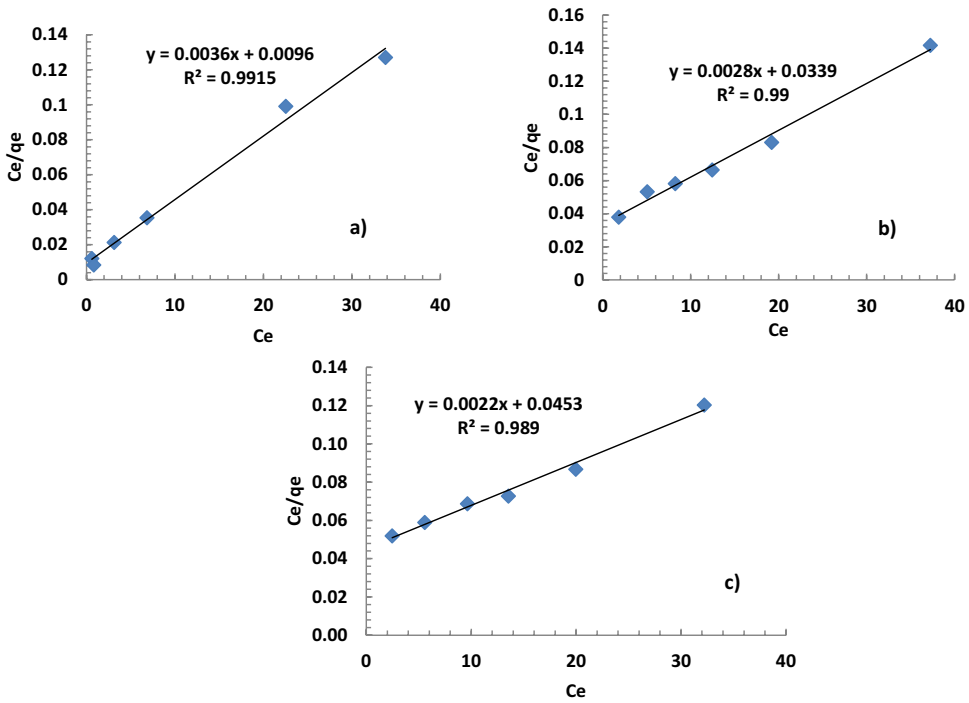

Fig. 4 Langmuir isotherm plots obtained for the adsorption of MB onto (**a**) AC of AC impregnated with 0.5 g Ag **d**) of AC impregnated with 1.0 g Ag (temperature: 25 °C, pH: 8, adsorbent dose: 0.1 g/100 mL, initial MB concentration: 50–300 mg $L.^{-1}$)

and 1.0 g Ag-impregnated ACs are shown in Fig. 6a-b and Table 4.

Table 4 shows the results of kinetic studies with AC, AC/Ag-0.5, and AC/Ag-1.0 samples. For three samples, it was seen that the most compatible model was the pseudo-second-order kinetic model with a temperature of 298 K and an R^2 value of 0.99. In addition, the qe values calculated because of the experiments (the amount of adsorbed substance) and the qe values calculated using the pseudo-second order kinetic model are compatible with each other.

These results were indicated that the adsorption of MB by AC, AC/Ag-0.5, and AC/Ag-1.0 it confirms of its chemical adsorption model of the pseudo-two-stage and also assumes that the adsorption rate was controlled by chemical adsorption (Wang et al. 2022).

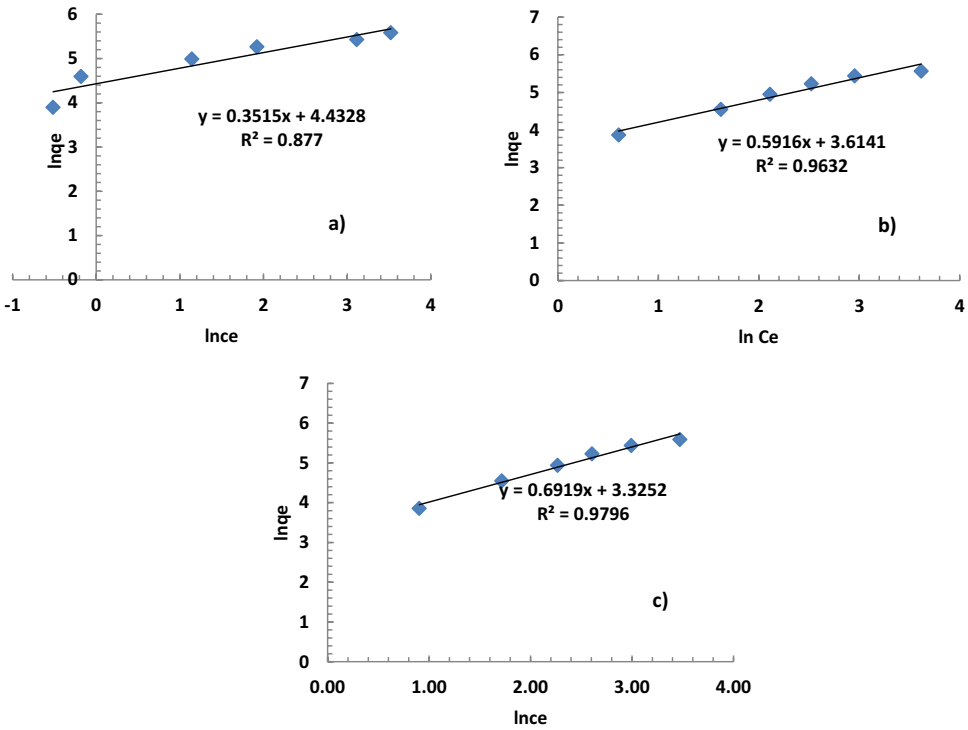

Fig. 5 Freundlich isotherm plots obtained for the adsorption of MB onto (**a**) AC, **b**) of AC impregnated with 0.5 g Ag, **c**) of AC impregnated with 1.0 g Ag (temperature: 25 °C, pH: 8, adsorbent dose: 0.1 g/100 mL, initial MB concentration: 50–300 mg $L.^{-1}$)

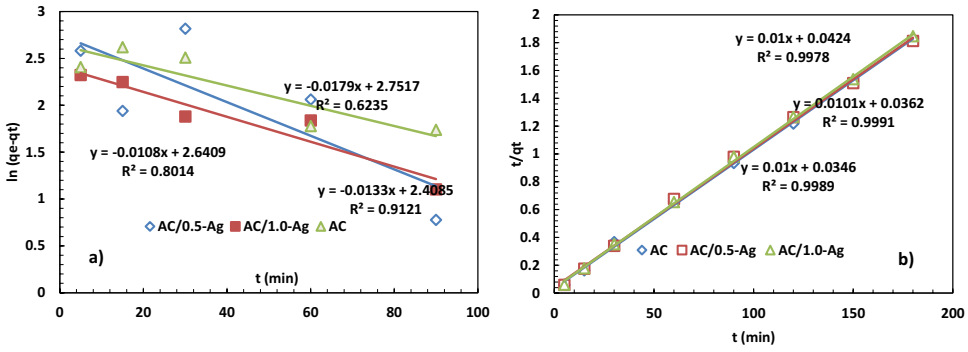

Fig. 6 Pseudo first-order kinetic modeling results obtained for MB adsorption onto AC, AC impregnated with 0.5 g Ag and AC impregnated with 1.0 g Ag, **b**) pseudo second-order kinetic results obtained for MB adsorption onto AC, AC impregnated with 0.5 g Ag and AC impregnated with 1.0 g Ag (initial MB concentration: 100 mg/L, adsorbent dose: 0.1 g/100 mL, pH: 8, temperature: 298 K)

Table 4 Kinetic results are determined based on pseudo first and second-order kinetic models

Sample	Pseudo first order			Pseudo second order			
	$q_{e\,exp}$	$k_{1,\,min}{}^{-1}$	q_{ecal}(mg g^{-1})	R^2	k_2 (g.mg^{-1}.min^{-1})	q_{ecal} (mg g^{-1})	R^2
AC	98.46	0.179	15.66	0.62	0.29	100	0.99
AC/0.5-Ag	99.34	0.011	14.03	0.80	0.28	99.00	0.99
AC/1.0-Ag	97.50	0.013	1.12	0.91	0.29	100.00	0.99

Desorption of MB from AC, AC/Ag-0.5, and AC/Ag-1.0

Desorption work is important in terms of reducing the cost of water when used in industrial applications owing to the reuse of the material. The desorption of adsorbents AC, AC/Ag-0.5, and AC/Ag-1.0 was investigated after loading the adsorbent with 100 mL of 100 mg L-1 MB. HCl solution with 0.01, 0.1, and 0.5 M concentrations were used for desorption and the adsorbents were obtained as 87%, 92%, and 96% respectively for AC. For AC/Ag-0.5 adsorbent was obtained as 91%, 95%, and 97% and for AC/Ag-1.0 to be 92%, 95%, and 98%. These results designated that the desorption process was higher when activated carbon was coated with Ag^+.

It is also shown that it is suitable for adsorption and removal of MB from aqueous solutions. Table 5 shows the comparison of MB adsorption capacities with different adsorbents in the literature.

Determination of antibacterial properties of silver-coated activated carbons

The disk diffusion method was used to determine the qualitative antibacterial properties of silver nanoparticle-bound AC (Xin et al. 2005). The study was conducted with two types of bacteria, gram-negative *E. coli* and gram-positive *S. aureus*. The antibacterial properties of AC and silver nanoparticle bonded activated carbon were compared. As can be seen in Fig. 6, there was no inhibition area against *E. coli* and *S. aureus* bacterial cultures around the activated carbon, but the activated carbon with silver nanoparticles showed an antibacterial effect against both bacterial species.

The strength of the antibacterial property of AgNPs differs in Gram-positive and -negative bacteria. This is may be due to species differ in their cell walls' architecture, thickness, and composition (Tamayo et al. 2014). It is known that *E. coli*, a Gram-negative bacterium, is more sensitive to Ag^+ ions than Gram-positive *S. aureus*. The reason for the different sensitivity lies in peptidoglycan, an important component of the bacterial cell membrane. In Gram-positive bacteria, the cell wall consists of a negatively charged peptidoglycan layer about 30 nm thick whereas in Gram-negative bacteria there is only a 3 to 4 nm peptidoglycan layer. These structural differences, including the thickness and composition of the cell wall, explain why Gram-positive S aureus is less sensitive to AgNPs and Gram-negative *E. coli* (Fayaz et al. 2010; Espinosa-Cristobal et al. 2009).

In the study in which we investigated the antimicrobial properties of AgNPAC, the findings showed that it inhibited *S. aureus* and *E. coli* in different zone ranges, as seen in Table 4. Results were evaluated concerning EUCAST disc diffusion results (2019). Ampicillin (10 mg) and Cefotaxime (30 mg).

Note: Most coagulase-negative staphylococci are penicillinase producers and many are resistant to ampicillin and methicillin (EUCAST, 2019).

Due to its reactive electronic structure, the silver ion joins the donor groups containing sulfur, oxygen, and nitrogen. These three compounds, in which the silver ion is added, are found in biological molecules as amino, imidazole, carboxylate, and phosphate groups (Duran et al. 2007). Thus, silver ion reacts with thiol groups and causes the inactivation of bacteria. The silver ion also causes the formation of hydrogen peroxide, which catalyzes the destructive oxidation of microorganisms. Silver ions and hydrogen peroxide destroy protein cells. Since the antibacterial effect of silver ions is directly proportional to Ag^+ concentration, silver ions are likely to dominate more than one target, such as DNA or cellular proteins (Prakash et al. 2013). Our study also observed that the antibacterial effect of the materials increased as the silver ion concentration increased (Table 6).

Today, several different chlorine-based methods are used to disinfect drinking water, and pathogens in drinking water are efficiently inhibited. However, some natural organic substances (NOM) in water can combine with iodide and bromide and turn into some harmful carcinogenic disinfection by-products (DBPs) (Richardson et al. 2007; Nieuwenhuijsen et al. 2009). However, due to the volatile nature of the chlorine, which is frequently used in drinking water

Table 5 Comparison of MB adsorption capacity of different kinds of adsorbents reported in the literature

Activating reagent	Adsorbent	*qmax* (mg /g)	Isotherm	Adsorption kinetic	Ref
$ZnCl_2$	*Citrullus lanatus* Rind (AC)	231.48	Langmuir	Pseudo-second order	Uner et al. 2016
$ZnCl_2$	Catalpa acbignonioides (AC)	271.00	Langmuir	Pseudo-second order	Uner et al. 2017
$ZnCl_2$	*Elaeagnus stone*	925.9	Langmuir	Pseudo-first order	Geçgel and Uner 2018
-	Ag–NP–AC	75.02	Langmuir	Pseudo-second order	Ghaedi et al. 2018
-	AgNPs-AC	172.22	Langmuir	Pseudo-first and second order	Van et al. 2018
H_3PO_4	Hazelnut-activated carbon (AC)	277.77	Langmuir	Pseudo-second order	This study
H_3PO_4	AC/0.5- Ag	357.14	Langmuir	Pseudo-second order	This study
H_3PO_4	AC/1.0- Ag	454.54	Langmuir	Pseudo-second order	This study

Table 6 Inhibition zone diameters of *S. aureus* (ATCC 25,923) and *E. coli* (ATCC 25,922)

Nano composites	Dose(mg)	Zon inhibasyon (mm)		Reference
		S. aureus	*E. coli*	
AgAC(SA)		8.2	9.1	Saravanan et al. 2016
AgAC(UA)		12.0	8.0	Saravanan et al. 2016
AgNPs		13.3	15.5	Njue et al. 2020
BCAg-0.5 g		11.4	12.6	Yang et al. 2009
BCA-1 g		11.5	12.6	Yang et al. 2009
AgNP-AC		17–18		Karthik and Radha 2016
ACNP		20		Varghese et al. 2013
ACF-Ag30			11.8	Yoon et al. 2008
Ag-AC NC		15	15	Devi et al., 2019
AgNPs/AC-CNF		6	5.8	Sobhan et al. 2020
AgNPAC		13.38	10.60	Karadirek and Okkay 2019
AC/Ag			2.8	
AgNP/AC		6–19	6	Taha et al. 2020
AC	10 mg	0	0	This study
0.5gAgNPAC	10 mg	23.2	18.3	This study
1 g AgNPAC	10 mg	34.1	24.1	This study
Ampicillin	10 mg	43.1	15.2	This study
Sefotaksim	30 mg	22.8	31.3	This study

treatment, the chlorine concentration may decrease over time in the waters that are kept as treated in the tanks, and several microbial growths may occur again in the waiting water in the absence of chlorine in the environment (Krantzberg et al. 2010). On the other hand, systems using UV in drinking water disinfection are quite high in terms of cost. NOMs in drinking water provide the formation of some harmful DBPs in disinfection with UV (Choi and Choi 2010; Dotson et al. 2010). Although it is used for water disinfection in reverse osmosis membranes, it is not often preferred because it causes biological contamination in long-term use and membrane modules are very costly (Biswas and Bandyopadhyaya 2016). Maybe evaluation of the disinfection techniques with NPAgACs will be new approaches to obtain low-cost and safe drinking water for public health.

The time optimization of the antibacterial treatment

Optimization of the antibacterial effect of *E. coli* bacteria against time is shown in Fig. 7. It shows that the antibacterial effect changes with the increase in the bacteriostatic time on the AC/Ag composite. While AC/Ag composite bacteriostatic time was 30 min, its antibacterial rate was over 90%. It showed that the optimal bacteriostatic time was 30 min.

As seen in Fig. 7, it was not taken into account because more than 300 colonies grew in the zeroth and tenth-min sowings, and less than thirty min in the fortieth min. By the 20th min, significant colony reduction was observed, and

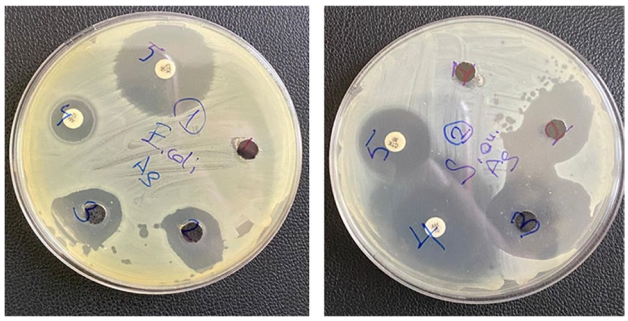

Fig. 7 Antibacterial activity of activated carbon and silver nanoparticle bonded activated carbon against *E. coli* and *S. aureus* bacteria

only one colony was observed at the fortieth min. In this study, 10^5 CFU/mL of *E. coli* was completely inhibited in 30 min. The same protocol was performed for 10^5 CFU/mL of *E. coli* with AC only (without Ag) and no reduction was observed within 40 min. While Zhao et al. (2013) removed *E. coli* from drinking water in 120 min in a similar study with AgAC, Yoon et al. (2008) reported the time taken for *E. coli* to be destroyed by AgAC as 60 min. Biswas and Bandyopadhyaya (2016), on the other hand, reported that all *E. coli* of 10^4 CFU/mL in drinking water were destroyed within 25 min of contact with the filter made with AgAC (Yoon et al. 2008; Zhao et al. 2013; Biswas and Bandyopadhyaya 2016) (Fig. 8).

Calculation of the number of colonies is carried out by taking into account the dilution carried out before sowing.

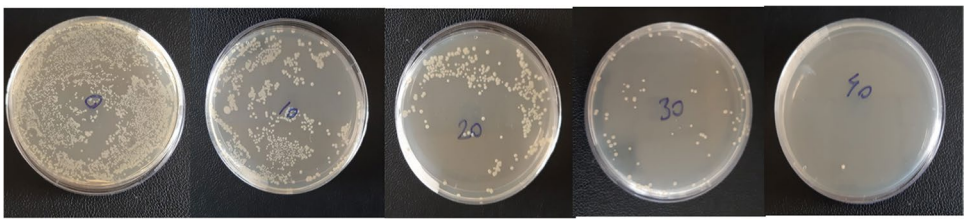

Fig. 8 The antibacterial effect changes with the increase in the bacteriostatic time on the AC/Ag composite

In this case, while our initial colony count was 10^8 CFU/mL, this number was also taken into account in the counting, since the first treatment was started with 10^5 CFU/mL colonies at the end of three dilutions. CFU was calculated using Eq. (7) (Gamazo et al. 2005).

$$\frac{(CFU)}{\mathrm{mL}} = \frac{(\mathrm{No.of\,colonies})\mathrm{x}(\mathrm{dilution\,factor})}{\mathrm{volume\,of\,culture\,plate}} \quad (7)$$

In drinking water with an initial concentration of 10^5 CFU/ml, all cells were killed within 30 min at the end of the treatment. As a result, 10^5 CFU/mL of *E. coli* bacteria was destroyed with 5 logarithmic reductions by using AgNPAC 30 min after treatment.

The recommended maximum limit for the presence of Ag ions in drinking water is 100 µg/L (Levard et al. 2013). It is known that the presence of chlorine, which is used to disinfect drinking water, significantly affects the release of Ag ions on NPAgAC into the water. However, some research was reported that no Ag ions were found in drinking water treated with NPAgAC for a long time (15 days). It has been reported that the use of NPAgAC, especially in systems treated with a continuous flow system, does not pose a risk in terms of Ag release (Biswas and Bandyopadhyaya 2016).

Conclusions

Nowadays, as environmental wastes increase, there is a search for evaluation of these wastes in different areas. In this context, activated carbon is one of the favorite materials with many application areas. Therefore, in this study, hazelnut shell, which is an easy and cost-effective material with a lot of waste in our country, was preferred. According to the results of the brief analysis, the low ash (1.3%), high volatile matter (64.91%), and fixed carbon (26.56%) content of the hazelnut shell support that the hazelnut shell is a suitable raw material to produce activated carbon. In addition, considering the criteria such as storage life, footprint, applicability, productivity, and surface area, which are important parameters to be considered in the selection of raw materials for the low-cost activated carbon production, it has been determined that the hazelnut shell is a suitable material for production. An AC-Ag composite containing nano-silver was synthesized by the reduction method. Structural properties of hazelnut shell, AC, and silver-coated activated carbons were analyzed by FT-IR, SEM/EDS, XRD, and BET. Experimental equilibrium data obtained for MB adsorption were applied to Langmuir and Freundlich isotherm models. The maximum adsorption capacities (q_{max}) of AC calculated from the linear Langmuir isotherm equation, AC impregnated with 0.5 g Ag and AC impregnated with 1.0 g Ag are 277.77, 357.14, and 454.54 mg g^{-1}, respectively. When the R^2 values of the first and second-order kinetic models were examined, it was found that the adsorption rate of MB on AC-Ag nanocomposite surfaces at 25 °C was in better agreement with the second-order kinetic model. Silver-coated AC showed excellent bacteriostatic activity against *E. coli* and *S. aureus*. The results show that the composite has good prospects for applications in drinking water. Since Ag particles directly blocked the pores in activated carbon, BET surface area, total pore volume and average pore diameter of ACs/Ag composites decreased as the amount of Ag increased. The smaller reduction in surface area is why this material is promising in environmental and antibacterial studies.

Author contribution Birsen Arıcı contributed to the design and execution of the experiments and calculation of the data. Assoc. Dr. Esra Altintig contributed to the visualization, interpretation, supervision, and editing of the experiments. Prof. Dr. Sukru Karatas contributed to supervision and editing.

Funding This research is partially funded by Sakarya University of Applied Sciences and Istanbul Aydın University.

Data availability The data that support the findings of this study are openly available on request.

Declarations

Ethics approval The manuscript has not been submitted to more than one journal for simultaneous consideration. No data, text, or theories by others are presented in our manuscript.

Consent to participate We do not have any person's data in any form. Consent for publication We do not have any individual person's data in any form.

Consent for publication Not applicable.

Competing interests The authors declare no competing interests.

References

Al Bahri M, Calvo L, Gilarranz M, Rodríguez JJ (2012) Activated carbon from grape seeds upon chemical activation with phosphoric acid: application to the adsorption of diuron from water. Chem Eng J 203:348–356

Altintig E, Kirkil S (2016) Preparation and properties of Ag-coated activated carbon nanocomposites produced from wild chestnut shell by $ZnCl_2$ activation. J Taiwan Inst Chem Eng 63:180–188

Altintig E, Arabaci G, Bilgin S (2013) Preparation and antibacterial activity of silver coated activated carbon from rice husks. Res J Biotech 8(9):17–21

Altintig E, Alsancak A, Karaca H, Angın D, Altundag H (2022) The comparison of natural and magnetically modified zeolites as an adsorbent in methyl violet removal from aqueous solutions. Chem Eng Commun 209(4):555–569

Altıntıg E, Acar I, Altundag H, Ozyıldırım O (2015) Production of activated carbon from rice husk tosupport Zn^2+ ions. Fresenius Environ Bull 24(4):1499–1506

Angın D (2014a) Utilization of activated carbon produced from fruit juice industry solid waste for the adsorption of Yellow 18 from aqueous solutions. Bioresource Technol 168:256–266

Angın D (2014b) Production and characterization of activated carbon from sour cherry stones by zincchloride. Fuel 115:804–811

Benaddi H, Bandosz TJ, Jagiello J, Schwarz JA, Rouzaud JN, Ledras D, Beguin F (2000) Surface functionality and porosity of activated carbons obtained from chemical activation of wood. Carbon 38:669–674

Berrios M, Martı´n MA, Martı´n A (2012) Treatment of pollutants in wastewater: Adsorption of methylene blue onto olive-based activated carbon. J Ind Eng Chem 18:780–784

Biswas P, Bandyopadhyaya R (2016) Water disinfection using silver nanoparticle impregnated activated carbon: Escherichia coli cell-killing in batch and continuous packed column operation over a long duration. Water Res 100:105–115

Budinova T, Ekinci E, Yardım F, Grimm A, Björnbom E, Minkova V, Goranova M (2006) Characterization and application of activated carbon produced by H_3PO_4 and water vapor activation. Fuel Proc Techn 87:899–905

Chaudhari VR, Haram SK, Kulshreshtha SK, Bellare JR, Hassan PA (2007) Micelle assisted morphological evolution of silver nanoparticles. Colloids Surf a: Physicochem Eng Asp 301(13):475–480

Choi Y, Choi YJ (2010) The effects of UV disinfection on drinking water quality in distribution systems. Water Res 44(1):115–122

Dang TMD, Le TTT, Fribourg-Blanc E, Dang MC (2011) Synthesis and optical properties of copper nanoparticles prepared by a chemical reduction method. Adv Nat Sci: Nanosci Nanotechnol 2(1):015009

Danish M, Hashim R, Ibrahim MNM, Sulaiman O (2013) Effect of acidic activating agents on surfacearea and surface functional groups of activated carbons produced from Acacia mangium wood. J Anal Appl Pyrolysis 104:418–425

Devi TB, Mohanta D, Ahmaruzzaman M (2019) Biomass derived activated carbon loaded silver nanoparticles: aneffective nanocomposites for enhanced solar photocatalysis and antimicrobial activities. J Ind Eng Chem 76:160–172

Dinu MV, Dragan ES (2010) Evaluation of Cu^{2+}, Co^{2+} and Ni^{2+} ions removal from aqueous solution using a novel chitosan/clinoptilolite composite: kinetics and isotherms. Chem Eng J 160:157–163

Dotson AD, Metz D, Linden KG (2010) UV/H_2O_2 treatment of drinking water increases post-chlorination DBP formation. Water Res 44(12):3703–3713

Duran N, Marcarto PD, De Souza GIH, Alves OL, Esposito E (2007) Antibacterial effect of silver nanoparticles produced by fungal process on textile fabrics and their effluent treatment. Jbiomed Nanotechnol 3:203–208

Espinosa-Cristobal LF, Martinez-Castanon GA, Martinez-Martinez RE, Loyola-Rodriguez JP, Patino-Marin N, Reyes-Macias JF (2009) Antibacterial effect of silver nanoparticles against Streptococcus mutans. Mater Lett 63:2603–2606

Fayaz M, Balaji K, Girilal M, Yadav R, Kalaichelvan PT, Venketesan R (2010) Biogenic synthesis of silver nanoparticles and its synergetic effect with antibiotics: a study against Gram positive and Gram-negative bacteria. Nanomedicine 6:103–109

Feng QL, Wu J, Chen GQ, Cui FZ, Kim TN (2000) A mechanistic study of antibacterial effects of silver ions on Escherichia Coli and Staphylococcus aureus. J Biomed Mater Res 52(4):662–668

Fischer C, Oschatz M, Nickel W, Leistenschneider D, Kaskel S, Brunner E (2017) Bioinspired carbide-derived carbons with hierarchical pore structure for the adsorptive removal of mercury from aqueous solution. Chem Commun 53:4845–4848

Gamazo C, Lopez-Gani I, Diaz R (2005) Manual practico de microbiologia. Elsevier, Spain, p 231

Gao Y, Yue Q, Gao B, Sun Y, Wang W, Li Q, Wang Y (2013) Preparation of high surface area-activated carbon from lignin of papermaking black liquor by KOH activation for Ni(II) adsorption. Chem Eng J 217:345–353

Gao S, Wang Z, Wang H, Jia Y, Xu N, Wang X, Wang J, Zhang C, Tian T, Shen W (2022) Peroxydisulfate activation using B-doped biochar for the degradation of oxytetracycline in water. Appl Surf Sci 599:153917

Gecgel U, Kocabıyık B, Uner O (2015) Adsorptive removal of methylene blue from aqueous solution by the activated carbon obtained from the fruit of catalpa bignonioides. Water Air Soil Pollut 226:238

Geçgel U, Uner O (2018) Adsorption of bovine of serum albümin onto activated carbon prepared from *elaeagnus* stone. Bull Chem Soc Ethiop 32(1):53–63

Ghaedi M, Roosta M, Ghaedi AM, Ostovan A, Tyagi I, Agarwal S, Gupta VK (2018) Removal of methylene blue by silver nanoparticles loaded on activated carbon by an ultrasound-assisted device: optimization by experimental design methodology. Res Chem Intermed 44:2929–2950

Hadoun H, Sadaoui Z, Souami N, Sahel D, Toumert I (2013) Characterization of mesoporous carbon prepared from date stems by H_3PO_4 chemical activation. Appl Surf Sci 280:1–7

Hameed BH, Ahmad AA, Aziz N (2007) Isotherms, kinetics, and thermodynamics of acid dye adsorption on activated palm ash. Chem Eng J 133(1–3):195–203

Han R, Ding D, Xu Y, Zou W, Wang Y, Li Y, Zou L (2008) Use of rice husk for the adsorption of congo red from aqueous solution in column mode. Bioresour Technol 99(8):2938–2946

Hassan M, Abou-Zeid R, Hassan E, Berglund L, Aitomäki Y, Oksman K (2017) Membranes based on cellulose nanofibers and activated carbon for removal of Escherichia coli bacteria from water. Polymers 9(8):335

Hayashi JI, Horikawa T, Takeda I, Muroyama K, Ani FN (2002) Preparing activated carbon from various nutshells by chemical activation with K_2CO_3. Carbon 40(13):2381–2386

Hulton G, World Health Organization (2012) Global costs and benefits of drinking-water supply and sanitation interventions to reach the MDG target and universal coverage (No. WHO/HSE/WSH/12.01). World Health Organization

Jawad AH, Ismail K, Ishak MAM, Wilson LD (2019) Conversion of Malaysian low-rank coal to mesoporous activated carbon: structure characterization and adsorption properties. Chin J Chem Eng 27(7):1716–1727

Jiun-Horng T, Hsiu-Mei C, Guan-Yinag H, Hung-Lung C (2008) Adsorption characteristics of acetone, chloroform, and acetonitrile on the sludge-derived adsorbent, commercial granular activated carbon and activated carbon fibers. J Hazard Mater 154:1183–1191

Karadirek S, Okkay H (2019) Ultrasound assisted green synthesis of silver nanoparticle attached activated carbon for levofloxacin adsorption. J Taiwan Inst Chem Eng 105:39–49

Kazemi SPH, Dehhaghi M, Ok YS, Nizami AS, Khoshnevisan B, Mussatto SI, Aghbashlo M, Tabatabaei M, Lam SS (2020) A comprehensive review of engineered biochar: production, characteristics, and environmental applications. J Clean Prod 270:122462

Kazmi SJ, Shehzad MA, Mehmood S, Yasar M, Naeem A, Bhatti AS (2014) Effect of varied Ag nanoparticles functionalized CNTs on its anti-bacterial activity against *E. coli*. Sens Actuators, A 216:287–294

Khuluk RH, Rahmat A (2019) Removal of methylene blue by adsorption onto activated carbon from coconut shell (Cocous nucifera L). Indones J Sci Technol 4(2):229–240

Krantzberg G, Tanik A, do Carmo JSA, Indarto A, Ekdal A, Gurel M, Mantas PE, Wang Z, Wang G, Zhao C, Machiwal D, Jha MK, Lin R, Huang X, Zhang X, Wang W, Chuai X, Li G (2010) Advances in water quality control. Scientific Research Publishing. Inc. USA 2(3):41

Kumar A, Vemula PK, Ajayan PM, John G (2008) Silver nanoparticle embedded antimicrobial paintsbased on vegetable oil. Nat Mater 7:236–241

Levard C, Mitra S, Yang T, Jew AD, Badireddy AR, Lowry GV, Brown GE Jr (2013) Effect of chloride on the dissolution rate of silver nanoparticles and toxicity to E. coli. Environ Sci Technol 47(11):5738–5745

Lima EC, Hosseini-Bandegharaei A, Moreno-Piraj´an JC, Anastopoulos I (2019) A critical review of the estimation of the thermodynamic parameters on adsorption equilibria Wrong Use of Equilibrium Constant in the Van't Hoof Equation for Calculation of Thermodynamic Parameters of Adsorption. J Mol Liq 273:425–434. https://doi.org/10.1016/j.molliq.2018.10.048

Mbarki F, Selmi T, Kesraoui A (2022) Mongi SeffeLow-cost activated carbon preparation from Corn stigmata fibers chemically activated using H_3PO_4, $ZnCl_2$ and KOH: Study of methylene blue adsorption, stochastic isotherm and fractal kinetic. Ind Crops Prod 178:114546

Mishra PC, Patel RK (2009) Removal of lead and zinc ions from water by low cost adsorbents. J Hazard Mater 168:319–325

Mohan D, Sarswat A, Singh VK, Alexandre-Franco M, Pittman CU Jr (2011) Development of magnetic activated carbon from almond shells for trinitrophenol removal from water. Chem Eng J 172:111–1125

Morgan S, Vural N, Demiral H (2009) Preparation of high-surface-area activated carbons from paulownia wood by $ZnCl_2$ activation. Microporous Mesaporous Mater 122:189–194

Ng SWL, Yilmaz G, Ong WL, Ho GW (2018) One-step activation towards spontaneous etching of hollow and hierarchical porous carbon nanospheres for enhanced pollutant adsorption and energy storage. Appl Catal B 220:533–541

Nieuwenhuijsen MJ, Martinez D, Grellier J, Bennett J, Best N, Iszatt N, Vrijheid M, Toledano MB (2009) Chlorination disinfection by-products in drinking water and congenital anomalies:review and meta-analyses. Environ Health Perspect 117(10):1486–1493

Njue W, Kithokoi JK, Swaleh S, Mburu J, Mwangi H (2020) Green ultrasonic synthesis, characterization andantibacterial activity of silver and gold nanoparticles mediated by Ganoderma lucidum extract. J Appl Mater Sci Eng Res 4:41

Prahas D, Kartika Y, Indraswati N, Ismadji S (2008) Activated carbon from jackfruit peel waste by H_3PO_4 chemical activation: pore structure and surface chemistry characterization. Chem Eng J 140:32–42

Prakash P, Gnanaprakasam P, Emmanuel R, Arokiyaraj S, Saravanan M (2013) Green synthesis of silver nanoparticles from leaf exract of Mımusop elengi, Linn. For enhanced antibacterial activityagainst multi drug resistant clinical isolates. Colloids Surf b: Biointerfaces 108:255–259

Richardson SD, Plewa MJ, Wagner ED, Schoeny R, De Marini DM (2007) Occurrence, genotoxicity, and carcinogenicity of regulated and emerging disinfection by-products in drinking water: a review and roadmap for research. Mutat Res 636(1–3):178–242

Saeed MM, Ahmed M, Ghaffar A (2003) Adsorption profile of molecular iodine and iodine number of polyurethane foam. Sep Sci Tech 38:715–731

Saka C, Balbay A (2021) Oxygen and nitrogen-functionalized porous carbon particles derived from hazelnut shells for the efficient catalytic hydrogen production reaction. Biomass Bioenergy 149:106072

Sang J, Aisawa S, Hirahara H, Kudo T, Mori K (2016) Self-reduction and size controlled synthesis of silver nanoparticles on carbon nanospheres by grafting triazine-based molecular layer for conductivity improvement. Appl Surf Sci 364:110–116

Saravanan A, Kumar PS, Karthiga Devi G, Arumugam T (2016) Synthesis and characterization of metallicnanoparticles impregnated onto activated carbon using leaf extract of Mukia maderasapatna: Evaluation of antimicrobial activities. Microb Pathog 97:198–203

Singh M, Singh S, Prasad S, Gambhir IS (2008) Nanotechnology in medicine and antibacterial effect of silver nanoparticles. Digest J Nano Biostruc 3:115–122

Singh S, Bharti A, Meena VK (2014) Structural thermal. zeta potential and electrical properties of disaccharide reduced silver nanoparticles. J Mater Sci Mater Electron 25:3747–3752

Sobhan A, Muthukumarappan K, Wei L, Van Den Top T, Zhou R (2020) Development of an activated carbon-based nanocomposite film with antibacterial property for smart food packaging. Mater Today Commun 23:101124

Spessato L, Bedin KC, Cazetta AL, Souza IPAF, Duarte VA, Crespo LHS, Silva MC, Pontes RM, Almeida VC (2019) KOH-super activated carbon from biomass waste: Insights into the paracetamol adsorption mechanism and thermal regeneration cycles. J Hazard Mater 371:499–505. https://doi.org/10.1016/j.jhazmat.2019.02.102

Sych N, Trofymenko S, Poddubnaya O, Tsyba M, Sapsay V, Klymchuk D, Puziy A (2012) Porous structure and surface chemistry of phosphoric acid activated carbon from corncob. Appl Surf Sci 261:75–82

Tamayo LA, Zapata PA, Vejar ND, Azócar MI, Gulppi MA, Zhou X, Thompson GE, Rabagliati FM, Páez MA (2014) Release of silver and copper nanoparticles from polyethylene nanocomposites and their penetration into Listeria monocytogene. Mater Sci Eng C 40:24–31

Tuan TQ, Van Son N, Dung HTK, Luong NH, Thuy BT, Van Anh NT, Hai NH (2011) Preparation and properties of silver nanoparticles loaded in activated carbon for biological and environmental applications. J Hazard Mater 192(3):1321–1329

Ucar S, Erdem M, Tay T, Karagoz S (2009) Preparation and characterization of activated carbon produced from pomegranate seeds by $ZnCl_2$ activation. Appl Surf Sci 255:8890–8896

Uner O, Gecgel U, Bayrak Y (2016) Adsorption of methylene blue by an efficient activated carbon prepared from citrullus lanatus rind: kinetic, ısotherm, thermodynamic, and mechanism analysis. Water Air Soil Pollut 227:247

Uner O, Geçgel U, Kolancilar H, Bayrak Y (2017) Adsorptive removal of rhodamine B with activated carbon obtained from okra wastes. Chem Eng Commun 204:772–778

Uner O, Gecgel U, Bayrak Y (2019) Preparation and characterization of mesoporous activated carbons from waste watermelon rind by using the chemical activation method with zinc chloride. Arab J Chem 12:3621–3627

Uner O, Geçgel U, Avcu T (2021) Comparisons of activated carbons produced from sycamore balls, ripe black locust seed pods, and Nerium oleander fruits and also their H_2 storage studies. Carbon Lett 31:75–92

Üner O, Bayrak Y (2018) The effect of carbonization temperature, carbonization time and impregnation ratio on the properties of activated carbon produced from *Arundo donax*. Microporous Mesoporous Mater 268:225–234

Unicef (2017) Progress on drinking water, sanitation, and hygiene

Van HT, Nguyen TMP, Thao VT, Vu XH, Nguyen TV, Nguyen LH (2018) Applying activated carbon derived from coconut shell loaded by silver nanoparticles to remove methylene blue inaqueous solution. Water Air Soil Pollut 229:393

Varghese S, Kuriakose S, Jose S (2013) Antimicrobial activity of carbon nanoparticles isolated from naturalsources against pathogenic Gram-negative and Gram-positive bacteria. J Nanosci 213:457865

Wang S, Li L, We H, Zhu ZH (2005) Unburned carbon as a low cost adsorbent for treatment of methylene blue containing wastewater. J Colloid Interface Sci 292:336–343

Wang Z, Tian T, Xu K, Jia Y, Zhang C, Li J, Wang Z (2022) Removal of antimony(III) by magnetic MIL-101(Cr)-NH_2 loaded with SiO_2: optimization based on response surface methodology and adsorption properties. Chem Paper 76:2733–2745

Wu J, Yu HQ (2006) Biosorption of 2, 4-dichlorophenol from aqueous solution by phanerochaetechrysosporium biomass: isotherms, kinetics and thermodynamics. J Hazard Mater 137:498–508

Wu S, Huang J, Zhang F, Wu Q, Zhang J, Pang R, Wei X (2019) Prevalence and characterization of food-related methicillin-resistant Staphylococcus aureus (MRSA) in China. Front Microbiol 10:304–310

Xin B, Jing L, Ren Z, Wang B, Fu H (2005) Effects of simultaneously doped and deposited Ag on the photocatalytic activity and surface states of TiO_2. J Phys Chem B 109:2805–2809

Yang FC, Wu KH, Liu MJ, Lin WP, Hu MK (2009) Evaluation of the antibacterial efficacy of bamboo charcoal/silver biological protective material. Mater Chem Phys 113(1):474–479

Yoon KY, Byeon JH, Park CW, Hwang J (2008) Antimicrobial effect of silver particles on bacterial contamination of activated carbon fibers. Environ Sci Technol 42(4):1251–1255

Yorgun S, Yıldız D (2015) Preparation and characterization of activated carbons from Paulownia wood by chemical activation with H_3PO_4. J Taiwan Inst Chem E 53:122–131

Zhang SJ, Shao T, Bekaroglu SSK, Karanfil T (2009) Adsorption of synthetic organic chemicals by carbon nanotubes: effects of background solution chemistry. Water Res 44(6):2067–2074

Zhang F, Tao Y, Chen S, Lu Y (2015) Preparation and properties of the silver loaded activated carbon fibers. Fibers Polym 16(9):2003–2010

Zhang XF, Liu ZG, Shen W, Gurunathan S (2016) Silver nanoparticles: synthesis, characterization, properties, applications, and therapeutic approaches. Int J Mol Sci 17(9):1534

Zhao Y, Wang ZQ, Zhao X, Li W, Liu SX (2013) Antibacterial action of silver-doped activated carbon prepared by vacuum impregnation. Appl Surf Sci 266:67–72

Publisher's note Springer Nature remains neutral with regard to jurisdictional claims in published maps and institutional affiliations.

Springer Nature or its licensor holds exclusive rights to this article under a publishing agreement with the author(s) or other rightsholder(s); author self-archiving of the accepted manuscript version of this article is solely governed by the terms of such publishing agreement and applicable law.